JOURNAL OF MATERIALS SCIENCE **33** (1998) 535–547

A theoretical and experimental approach to the active-to-passive transition in the oxidation of silicon carbide

Experiments at high temperatures and low total pressures

B. SCHNEIDER, A. GUETTE, R. NASLAIN
Laboratoire des Composites ThermoStructuraux (UMR 47 CNRS-SEP-UB1), Domaine universitaire, 3 allée de La Boétie, 33600 Pessac, France
M. CATALDI, A. COSTECALDE
Société Européenne de Propulsion, Le Haillan, BP 37, 33165 Saint-Médard-en-Jalles, France

Active-to-passive oxidation transition in chemical vapour deposited β-SiC was investigated in the temperature range $1300 \leqslant T \leqslant 1700\,^{\circ}C$ under low total pressures ($100 \leqslant P_{tot} \leqslant 800$ Pa) and relatively high linear gas flow rates ($10 \leqslant V_{gas} \leqslant 60\ m\,s^{-1}$) by thermogravimetric analysis. For given T, P_{tot} and V_{gas}, the oxygen partial pressure at the transition, $P^{t}_{O_2}$, corresponds to the value where the mass-loss rate per unit area of the oxidized sample, $\mathscr{R}$, is maximum. Logarithms of $P^{t}_{O_2}$ are linear functions of reciprocal temperature for given P_{tot}, and V_{gas}. V_{gas} has a significant influence on the position of the transition $\log(P^{t}_{O_2})–T^{-1}$ line. $P^{t}_{O_2}$ is also slightly affected by an increase of P_{tot} from 100 Pa to 800 Pa. In passive oxidation at high temperatures ($> 1500\,^{\circ}C$), large bubbles form in the silica film which is then disrupted leading to a loss of material. In active oxidation, $\mathscr{R}$ significantly depends on V_{gas}: the kinetics is diffusion or mass transfer controlled under the conditions investigated in the present study. In both active and passive oxidation regimes, a mass loss of the test specimen is always observed; an explanation is proposed.

1. Introduction

To ensure that silicon carbide will efficiently protect a material (e.g. SiC/SiC, C/SiC or C/C composites) in given oxidizing environments, its own oxidation behaviour must be previously known. The oxidation of silicon carbide has already been extensively investigated [1, 2], particularly at atmospheric pressure. It usually leads to the formation of a silica layer which protects the material from further attack. However, at low oxygen partial pressures and very high temperatures, silicon carbide oxidizes in an active manner: the products are gaseous and the specimen undergoes an important mass loss. Active-to-passive oxidation transition of silicon carbide has been theoretically examined elsewhere [3, 4]. Passive oxidation is ascribed to the formation–deposition of a silica film ($SiO_{2(cond)}$) on the SiC specimen surface, whereas in active oxidation conditions, all the silicon-containing products are gaseous ($Si_{(g)}$, $SiO_{(g)}$, …).

The purpose of the present work was to observe and understand the oxidation phenomena of silicon carbide under low total pressure (100–800 Pa) and high-temperature conditions (1300–1600 °C).

2. Experimental procedure

This study was conducted on chemically vapour deposited (CVD) silicon carbide in the form of SiC coating fragments removed from graphite substrates. The samples were cut with a laser as $10 \times 15\ mm^2$ plates with an average thickness of about 1 mm. The specimens were polished on the two largest faces using 1 μm diamond paste to remove the remaining carbon on one face and to obtain a specimen that had well-defined geometrical dimensions and flat faces. The test specimens were then ultrasonically cleaned in acetone. The geometry of the specimens was chosen so that the sample surface evolved very little during an oxidation test: a mass loss of about 20% only led to a reduction of 4% of the SiC sample surface. Fig. 1 represents an XRD diagram of the sample. The different peak positions correspond to β-SiC (the blende type), the higher intensity of the (1 1 1) peak as compared to the theoretical relative values [5] indicates that (1 1 1) β-SiC crystalline planes are preferentially oriented parallel to the largest faces of the sample. Microprobe analysis of a sample cross-section shows a slight excess of silicon (51 at % Si, 49 at % C) as compared to the

0022–2461 © *1998 Chapman & Hall*

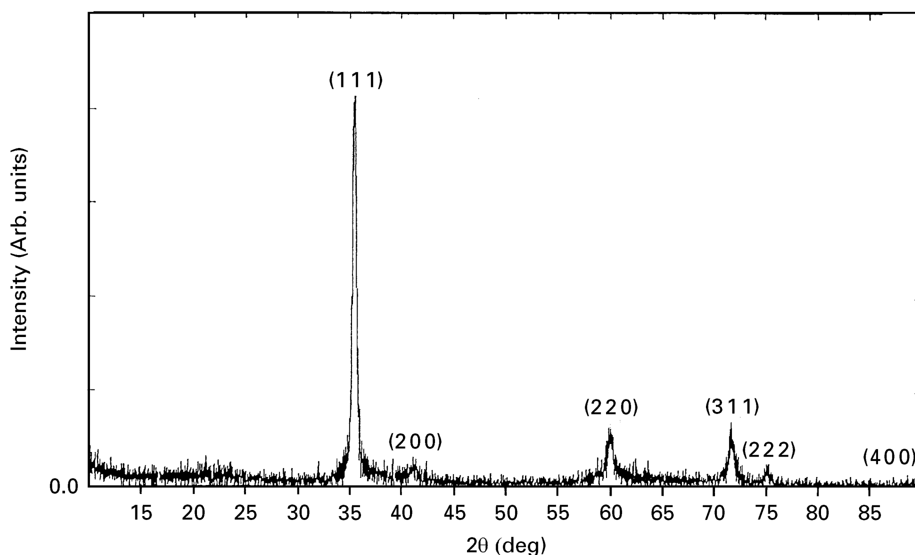

Figure 1 X-ray (CuK_α) diffraction spectrum of the CVD SiC substrate.

stoichiometric composition of silicon carbide. The density of the sample was 3.17 ± 0.07 g cm^{-3} as measured with an helium pycnometer (theoretical value 3.217 g cm^{-3}).

The oxidation furnace was equipped with a microbalance (Cahn microbalance, D101 series, sensitivity 1 μg) which was used to record the sample weight changes during the oxidation tests. The SiC specimen was hung on it using a zirconia rod and pin system which was designed to reduce the zirconia–SiC sample contact point surface in order to minimize or avoid possible reaction between the sample and its holder (as reported by Keys [6]). In addition, the specimen and its zirconia hanging system were weighed before and after the oxidation test (i) to control the weight change versus time data recorded throughout the test using a computer, and (ii) to ensure that the hanging system had a constant weight.

The sample chamber consisted of a 20 mm inner diameter alumina tube isolating the specimen from the heating system, i.e. the graphite susceptor and the inductor.

Mass flow controllers were used to measure and control the different reactant flow rates. High-purity argon (N56 argon, from Alphagaz, purity $\geqslant 99.9996\%$) and oxygen (N58 oxygen, from Alphagaz, purity $\geqslant 99.998\%$) were used to reduce as much as possible the influence of other gaseous reactant species (i.e. H_2O, CO, etc.). The reactant gas mixture was introduced into the furnace through the microbalance, circulating from top to bottom to avoid condensed oxide (silica) deposit on the sample holder (zirconia rod) which would have disturbed the sample weight change measurement.

A constant total pressure was maintained in the furnace using a pressure control system: it consisted of a capacitance manometer which provided measurements that were independent of gas composition, a throttle valve and a proportional, integral and derivative regulator.

The sample temperature was directly measured on the specimen surface. A two-colour optical pyrometer (Ircon Infrared Thermometers, R series, 24C05, uncertainty $< 10\,^\circ$C), which worked in the temperature range 900–2400 °C was used. The specimen was heated to the test temperature under flowing argon in about 0.5 h (at a rate of about 50 °C min^{-1}). At the end of the experiment, the SiC sample was cooled to room temperature under flowing argon in about 1 h (at a rate of 20–30 °C min^{-1}).

Because of the (highly temperature dependent) flow impingement on the specimen and its holder, temperature, total pressure and linear gas flow rate were held constant (independent of time) during the experiments carried out to determine the active-to-passive transition conditions. The signal delivered by the microbalance was, in that case, truly representative of the weight change of the oxidized specimen when the zirconia holder system weight had not changed.

The oxygen flow rate was increased, whereas the argon flow rate was decreased, in order to maintain a constant (independent of time) linear gas flow rate and to obtain the incoming gas mixture composition chosen for the first stage of the experiment. All these four parameters (T, P_{tot}, V_{gas} and $P^b_{O_2}$) were held at their as previously defined values for a time (between 10 min and several hours) that depended on the weight loss rate of the specimen. The oxygen content of the incoming gas mixture was then again increased and held at this higher value during stage 2. This process was repeated until the active-to-passive oxidation transition was thought to be overshot (or the weight loss of the SiC substrate became greater than 50%). When the highest $P^b_{O_2}$ stage was achieved and before cooling the test specimen, the oxygen flow was cut off and the argon flow rate conveniently increased to keep the total gas flow rate constant.

Auger electron spectroscopy (AES) and electron probe microanalysis (EPMA) were used to determine the SiC sample surface composition. When the weight change versus time curves did not allow the removal rate per unit area, $\mathscr{R}$, with sufficient precision, typically at 1300 °C ($\Delta m/m_0 \approx 0\%$), the active-to-passive oxidation transition point was defined using AES to

assess whether or not silica had been formed on the specimen during the oxidation experiment.

The conditions investigated in the present work were mainly chosen to determine a numerical model relating $\mathcal{R}$ to T, P_{tot}, $P^b_{O_2}$ and V_{gas}. They corresponded roughly to oxidizing environments that can be encountered by the thermal protective tiles of a space vehicle re-entering the Earth's atmosphere, i.e. high temperatures (1300–1700 °C) and low pressures (100–800 Pa). However, argon instead of nitrogen was used in the reactant gas mixture to avoid possible formation of silicon nitride [7, 8] in order to only focus on SiC oxidation.

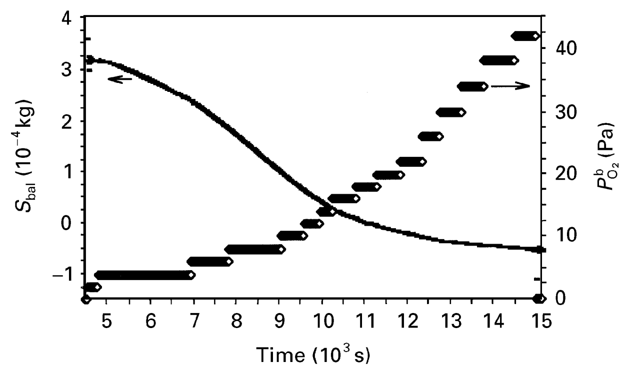

Figure 3 Oxidation for $T = 1500\,°C$, $P_{tot} = 500$ Pa and $V_{gas} = 25\ m\,s^{-1}$, weight change versus time of a CVD β-SiC plate.

3. Results and discussion
3.1. Active-to-passive oxidation transition

Fig. 2 shows a plot of the signal delivered by the microbalance, S_{bal}, versus time recorded during an oxidation test performed at 1500 °C, under 500 Pa total pressure and a total gas flow rate of about 25 ms^{-1}. The increase of S_{bal} observed for $t < 4000$ s and the decrease recorded for $15\,100\ s < t < 18\,200$ s only account for the change of flow impingement on the SiC specimen and its holder related to the change in temperature. When T, P_{tot} and V_{gas} are held constant at the different values chosen for the experiment (Fig. 3), S_{bal} is truly representative of the weight change of the sample, Δm. At each stage defined by fixed values of T, P_{tot}, V_{gas} and $P^b_{O_2}$, the weight of the SiC substrate decreases linearly with time. The plot of Δm versus time recorded during an experiment is thus divided into as many segments of a straight line as the number of $P^b_{O_2}$ conditions investigated in the test. The slopes of these lines are estimated by linear regression analysis. The weight loss rate per unit area, denoted $\mathcal{R}$ ($kg\,m^{-2}\,s^{-1}$), is derived from these values: it is equated to the ratio of this slope to the initial geometrical sample surface, S_0. The sample surface is not greatly affected by the oxidation test (i.e. $\Delta m/m_0 = 20\%$ corresponds to $\Delta S/S_0 \approx 4\%$), which explains the choice of S_0 in these calculations.

$\mathcal{R}$ increases rapidly with increasing $P^b_{O_2}$ (Fig. 4) until it reaches a maximum value and then progressively decreases when $P^b_{O_2}$ is further increased. Although mass loss is still observed during the last $P^b_{O_2}$ stage of the oxidation test, the surface of the oxidized sample after the experiment is covered with a silica film. Fig. 5 gives the composition profile determined by AES and ion sputtering of a sample oxidized at 1406 °C, 800 Pa, 10 $m\,s^{-1}$ and different $P^b_{O_2}$ stages, such that the last one corresponds to the domain where $\mathcal{R}$ decreases with increasing $P^b_{O_2}$. It typically shows a silica layer on the specimen surface indicating that the last $P^b_{O_2}$ stage(s) was conducted under passive oxidation conditions, despite the weight loss. Moreover, the kinetic energies of Auger electrons corresponding to silicon (Fig. 6) are slightly shifted towards lower energy values. This indicates that silicon is in an oxidized state revealing the existence of Si–O bonds, which is another proof of the existence of a silica layer on the sample surface. Fig. 7 represents a typical atomic profile of an SiC sample oxidized in conditions where $\mathcal{R}$ increases with $P^b_{O_2}$ ($T = 1600\,°C$, $P_{tot} = 100$ Pa,

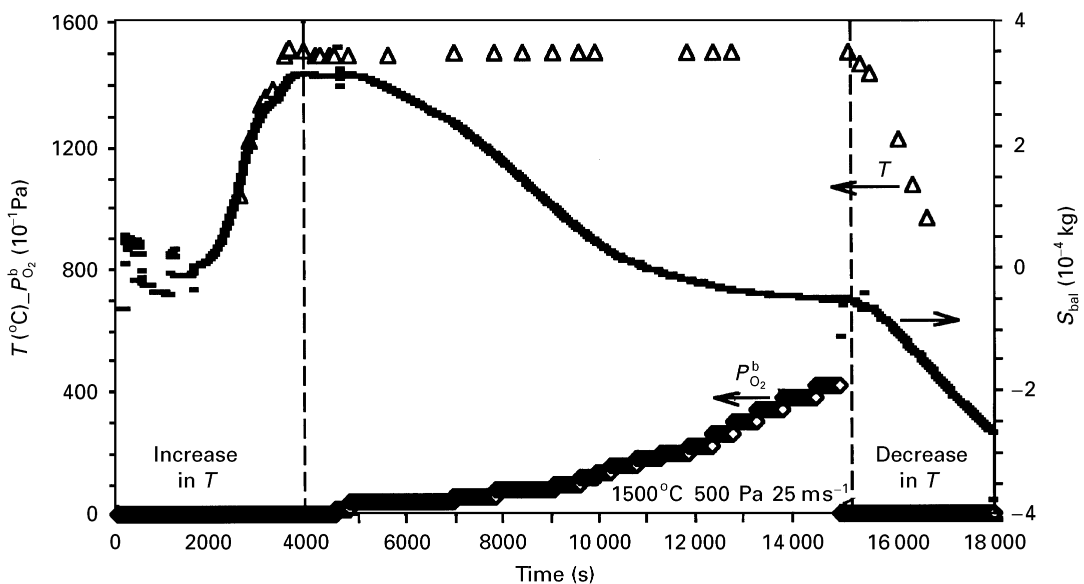

Figure 2 S_{bal}–time curve recorded during an oxidation test performed on a CVD β-SiC plate at 1500 °C, $P_{tot} = 500$ Pa, $V_{gas} = 25\ m\,s^{-1}$ and various $P^b_{O_2}$.

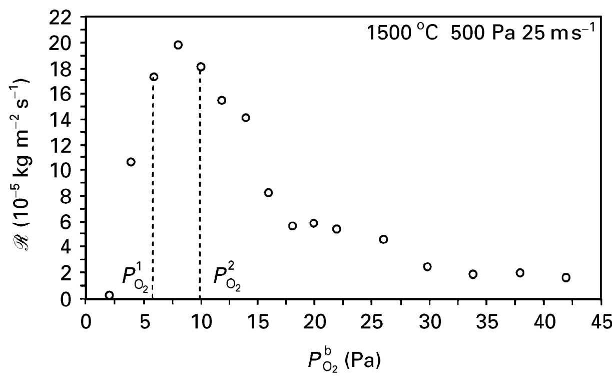

Figure 4 Mass loss rate per unit area versus oxygen partial pressure as derived from data of Fig. 3.

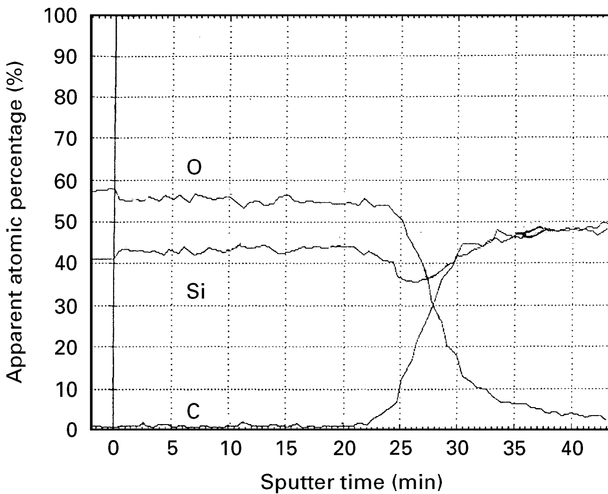

Figure 5 Composition profile determined by AES and argon ion sputtering of a SiC substrate oxidized at $T = 1406\,°C$, $P_{tot} = 800$ Pa, $V_{gas} = 10\ m\,s^{-1}$ and $P^b_{O_2} = 200$ Pa.

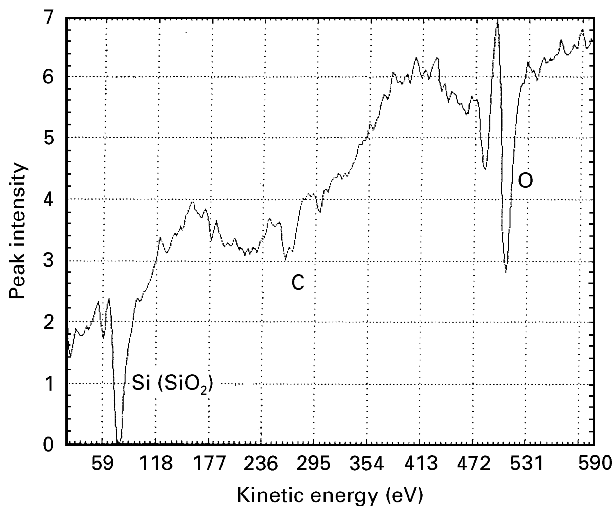

Figure 6 Kinetic energies of Auger electrons emitted by the surface of a SiC substrate oxidized at $T = 1500\,°C$, $P_{tot} = 500$ Pa, $V_{gas} = 25\ m\,s^{-1}$.

$V_{gas} = 60\ m\,s^{-1}$, $P^b_{O_2} \leqslant 15$ Pa). Here no oxide film is detected on the sample surface: the test specimen was oxidized in an active manner.

The oxygen partial pressure corresponding to the maximum value of $\mathscr{R}$ is therefore assigned to be characteristic of the active-to-passive oxidation transition.

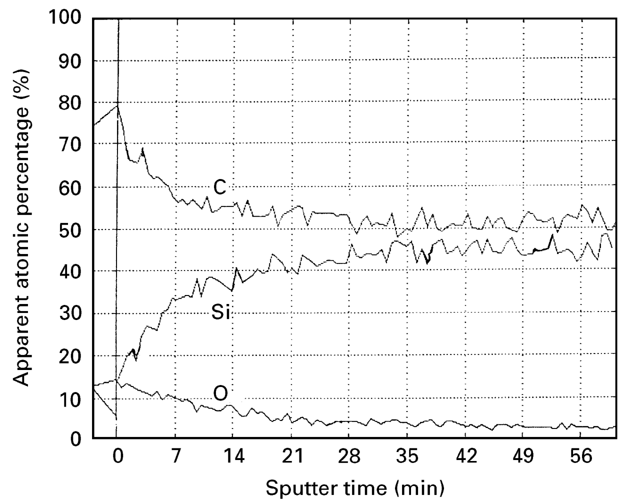

Figure 7 Composition profile determined by AES and argon ion sputtering (10 nm min^{-1} reference Ta_2O_5) of a SiC substrate oxidized at $T = 1600\,°C$, $P_{tot} = 100$ Pa, $V_{gas} = 60\ m\,s^{-1}$ and $P^b_{O_2} < 15$ Pa.

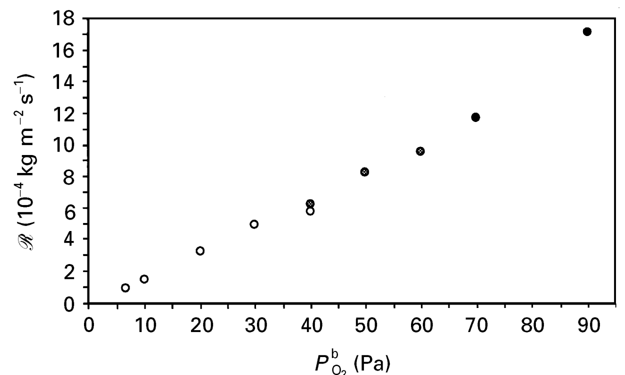

Figure 8 Oxidation of a SiC plate at $T = 1605\,°C$, $P_{tot} = 100$ Pa and $V_{gas} = 10\ m\,s^{-1}$. Weight loss rate per unit area versus oxygen partial pressure.

This value, denoted $P^t_{O_2}$ (where t stands for transition), has been experimentally determined for different T, P_{tot} and V_{gas} conditions. It belongs to the interval $[P^1_{O_2}; P^2_{O_2}]$ where $P^1_{O_2}$ and $P^2_{O_2}$ are the oxygen partial pressures of the two stages adjacent to the third one, where $\mathscr{R}$ has the greatest value. For instance, from Fig. 4, $P^t_{O_2}$ has a value greater than 6 Pa and lower than 10 Pa ($P^t_{O_2} = 8 \pm 2$ Pa) at 1500 °C, $P_{tot} = 500$ Pa and $V_{gas} = 25\ m\,s^{-1}$. In some cases (Fig. 8), $\mathscr{R}$ increases with $P^b_{O_2}$ until $P^b_{O_2} = P_{tot}$. No transition point can then be determined: it does not exist.

These results are listed in Table I and are shown in a $\log(P^b_{O_2}) = f(T^{-1})$ graph in Fig. 9. Vertical lines represent uncertainty (as indicated in Table I) in $P^t_{O_2}$ values.

In Fig. 10, experimental transition points are located in a $\log(P^b_{O_2}) - T^{-1}$ graph and compared to the theoretical limits of the "transition domain" previously determined [4]. Data obtained in the present work expand between the transition points of Rosner and Allendorf [9] and Hinze and Graham [10] and seem to be a direct continuity of those of Narushima *et al.* [11] (who are working at various low flow rates). All these experimental data belong to the "transition domain".

TABLE I Experimental $P^t_{O_2}$ transition points in the temperature range 1300–1605 °C

T (°C)	V_{gas} (m s^{-1})	P_{tot} (Pa)	$P^t_{O_2}$(Pa)
1300 (1573 K)	10	100	1 ± 1
1300 (1573 K)	10	800	1 ± 1
1400 (1673 K)	10	100	3 ± 3
1397 (1670 K)	60	100	1 ± 1
1406 (1679 K)	10	800	3 ± 3
1502 (1775 K)	10	100	11 ± 5
1503 (1776 K)	60	100	2 ± 1
1500 (1773 K)	25	500	8 ± 2
1504 (1777 K)	10	800	10 ± 3
1605 (1878 K)	10	100	Not observed
1602 (1875 K)	60	100	17 ± 3
1603 (1876 K)	10	800	45 ± 15

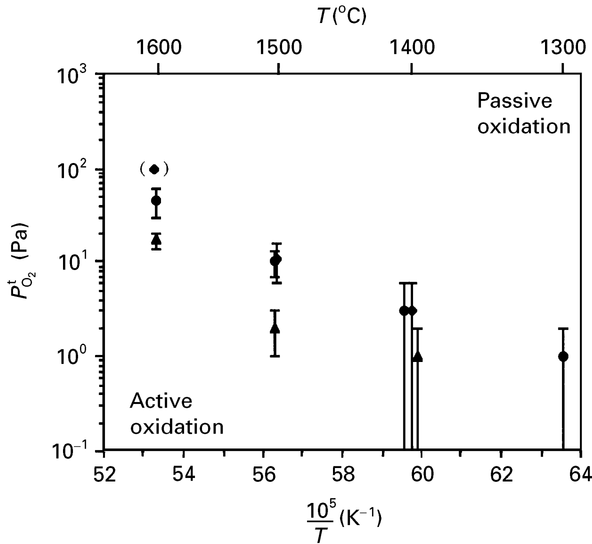

Figure 9 Oxygen partial pressure at transition versus reciprocal temperature. (◆) Transition point was not observed, (Table I). V_{gas} (m s^{-1})–P_{tot}(Pa): (◆) 10–100, (●) 10–800, (▲) 60–100.

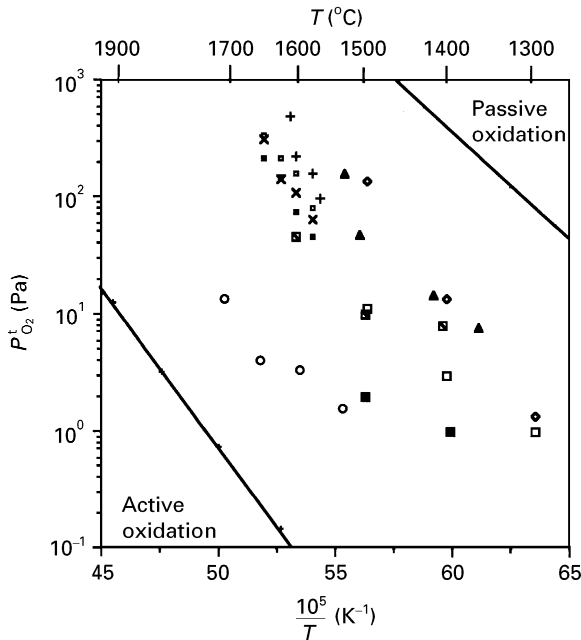

Figure 10 Oxygen partial pressure at transition versus reciprocal temperature. Comparison between reported experimental points [6, 9–11] and those determined, in the present work (PW) for various (P_{tot}–V_{gas}) conditions. The limits of the transition domain, previously determined [4], are indicated (—,—). (◇) [6], (▲) [10], (○) [9], (+ , □, ×, ■) [11], (□) PW 100–10, (⧅) PW 800–10, (■) PW 100–60.

3.2. Passive oxidation

3.2.1. Global mass loss

When Narushima *et al.* [11] or Gulbransen *et al.* [12] studied the active-to-passive transition in the oxidation of silicon carbide by TGA they observed a mass gain which was said to be characteristic of the oxidation in the passive mode. Here mass loss is observed in both active and passive oxidation regimes. The nature of the silica layer present on the test specimen surface can explain this behaviour. Depending on the experimental conditions, this layer can be discontinuous, poorly adherent to the SiC substrate and non-uniform in thickness. The main difference between the experimental conditions investigated in the literature [11, 12] and those examined in the present work, lies in the total pressure level. Narushima *et al.* [11] worked at atmospheric pressure (0.1 MPa) while the total pressure did not exceed a few hundred pascals in this study. At relatively high temperature, the silica film produced at the SiC/SiO_2 interface by oxidation of the SiC substrate can be significantly consumed by volatilization. Berton *et al.* [13] indicated that the vaporization of silica became noticeable above 1350 °C at a pressure of 1 kPa. The volatalization of the SiO_2 film occurs according to one of the following reactions

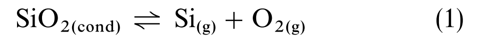

$$SiO_{2(cond)} \rightleftharpoons Si_{(g)} + O_{2(g)} \tag{1}$$

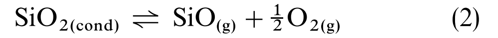

$$SiO_{2(cond)} \rightleftharpoons SiO_{(g)} + \tfrac{1}{2}O_{2(g)} \tag{2}$$

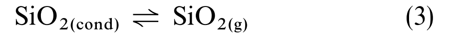

$$SiO_{2(cond)} \rightleftharpoons SiO_{2(g)} \tag{3}$$

The thickness of the SiO_2 scale (e_{SiO_2}) is ideally assumed to be uniform on the sample surface. It varies with time at a rate related to the mass loss rates per unit area due to (i) the consumption of the SiC substrate, $\mathscr{R}_{cons\,SiC}$, and (ii) the volatilization of the silica layer, $\mathscr{R}_{vol\,SiO_2}$, by the equation

$$\frac{de_{SiO_2}}{dt} = \frac{F_{SiO_2}}{\rho_{SiO_2}}\frac{M_{SiO_2}}{M_{SiC}}\mathscr{R}_{cons\,SiC} - \frac{1}{\rho_{SiO_2}}\mathscr{R}_{vol\,SiO_2} \tag{4}$$

where ρ_{SiO_2} is the SiO_2 density, M_{SiO_2} and M_{SiC} the molar weight of SiO_2 and SiC, respectively. The F_{SiO_2} factor accounts for the molar proportion of reacted SiC that has conducted to the formation of silica: it eliminates part of SiC that has reacted (with $O_{2(g)}$ or $SiO_{2(cond)}$ in contact) to form Si, SiO or SiO_2 gaseous species. The total mass gain per unit area of the overall sample, $\mathscr{R}_{glob}$, is equal to

$$\mathscr{R}_{glob} = \mathscr{R}_{form\,SiO_2} - \mathscr{R}_{vol.\,SiO_2} + \mathscr{R}_{form\,C} - \mathscr{R}_{vol\,C} - \mathscr{R}_{cons\,SiC} \tag{5}$$

In passive oxidation conditions (Fig. 5), $\mathscr{R}_{form\,C}$ is negligible (carbon is consumed in CO or CO_2 gaseous species when SiC is oxidized). So $\mathscr{R}_{form\,C}$ and $\mathscr{R}_{vol\,C}$ are assumed to be zero in Equation (5). Under steady-state conditions ($de_{SiO_2}/dt = 0$) when silica forms and evaporates at the same rate ($\mathscr{R}_{form\,SiO_2} \approx \mathscr{R}_{vol\,SiO_2}$), it follows that

$$\mathscr{R}_{glob} = \frac{-M_{SiC}}{F_{SiO_2}M_{SiO_2}}\mathscr{R}_{vol.\,SiO_2} \tag{6}$$

$\mathscr{R}_{\text{vol SiO}_2}$ and F_{SiO_2} are positive factors. $\mathscr{R}_{\text{glob}}$ is therefore negative under steady state conditions. Thus, when the SiO_2 film ideally assumed to be uniform on the sample surface, has reached its equilibrium critical thickness, $e^{\text{cr}}_{\text{SiO}_2}$, the specimen globally undergoes a mass loss proportional to $\mathscr{R}_{\text{vol SiO}_2}$. At a high fixed temperature (beyond 1350 °C), an increase in V_{gas} or a decrease in P_{tot} make the volatilization of the silica film easier, and thus lead to a greater mass loss rate of the sample.

In general, passive oxidation of silicon carbide is thought to be kinetically controlled by diffusion of (molecular or atomic) oxygen through the silica layer. Many authors [1,2] have proposed and experimentally validated parabolic laws as a consequence of this suggested mechanism. This means that $\mathscr{R}_{\text{cons SiC}}$ can be related to the molar flux of the oxygen through the silica layer, $J_{\text{O}_2,\text{ SiO}_2}$:

$$\mathscr{R}_{\text{cons SiC}} = C_{\text{reac}} M_{\text{SiC}} J_{\text{O}_2,\text{SiO}_2} \quad (7)$$

where C_{reac} indicates how many moles of SiC have reacted with 1 mol $O_{2(g)}$ to give silica and a carbonaceous product. C_{reac} depends on which reaction equation is considered and equals 1, $\frac{2}{3}$ or $\frac{1}{2}$ when the possible reaction equations are, respectively

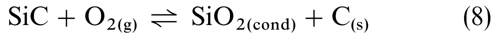

$$\text{SiC} + \text{O}_{2(\text{g})} \rightleftharpoons \text{SiO}_{2(\text{cond})} + \text{C}_{(\text{s})} \quad (8)$$

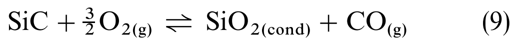

$$\text{SiC} + \tfrac{3}{2}\text{O}_{2(\text{g})} \rightleftharpoons \text{SiO}_{2(\text{cond})} + \text{CO}_{(\text{g})} \quad (9)$$

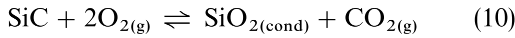

$$\text{SiC} + 2\text{O}_{2(\text{g})} \rightleftharpoons \text{SiO}_{2(\text{cond})} + \text{CO}_{2(\text{g})} \quad (10)$$

Assuming that (i) the oxygen partial pressure at the SiO_2/gas interface is equal to $P^{\text{b}}_{\text{O}_2}$, and (ii) Fick's first law can be applied, the molar flux of the O_2 molecule through the silica layer is given by

$$J_{\text{O}_2,\text{SiO}_2} = \frac{D_{\text{O}_2,\text{SiO}_2}(P^{\text{b}}_{\text{O}_2} - P^{\text{int}}_{\text{O}_2})}{RTe_{\text{SiO}_2}} \quad (11)$$

$D_{\text{O}_2,\text{SiO}_2}$ is the diffusion coefficient of oxygen in condensed silica film, $P^{\text{b}}_{\text{O}_2}$ and $P^{\text{int}}_{\text{O}_2}$ are the oxygen partial pressures in the bulk gas and at the SiC/SiO_2 interface, respectively. Equation 4 therefore becomes

$$\frac{\text{d}e_{\text{SiO}_2}}{\text{d}t} = \frac{F_{\text{SiO}_2} C_{\text{reac}} M_{\text{SiO}_2} D_{\text{O}_2,\text{SiO}_2}(P^{\text{b}}_{\text{O}_2} - P^{\text{int}}_{\text{O}_2})}{\rho_{\text{SiO}_2} RTe_{\text{SiO}_2}} - \frac{1}{\rho_{\text{SiO}_2}} \mathscr{R}_{\text{vol SiO}_2} \quad (12)$$

and the critical thickness of the silica layer (corresponding to steady state conditions: $\text{d}e_{\text{SiO}_2}/\text{d}t = 0$) is given by

$$e^{\text{cr}}_{\text{SiO}_2} = \frac{F_{\text{SiO}_2} C_{\text{reac}} M_{\text{SiO}_2} D_{\text{O}_2,\text{SiO}_2}(P^{\text{b}}_{\text{O}_2} - P^{\text{int}}_{\text{O}_2})}{RT\mathscr{R}_{\text{vol SiO}_2}} \quad (13)$$

In this expression, $\mathscr{R}_{\text{vol SiO}_2}$ is the only factor that depends on P_{tot} and V_{gas}. In addition, $e^{\text{cr}}_{\text{SiO}_2}$ is inversely proportional to the rate of volatilization of silica per unit area. At a given temperature and a fixed $P^{\text{b}}_{\text{O}_2}$, $e^{\text{cr}}_{\text{SiO}_2}$ therefore increases with increasing total pressure and/or decreasing V_{gas}. Working at high total pressure and low linear gas flow rate makes $e^{\text{cr}}_{\text{SiO}_2}$ large, and steady state conditions for the consumption of the SiC substrate are not rapidly reached and could not be observed during an experiment. In this case, the oxidation tests only give rise to a global mass gain of the specimen [11,12]. On the contrary, these results are inverted when working at very low total pressure and high linear gas flow rate and no mass gain is observed. This was the case for the conditions investigated in the present work ($P_{\text{tot}} = 100$–800 Pa and $V_{\text{gas}} = 10 - 60\ \text{m s}^{-1}$).

3.2.2. Bubble formation

Fig. 11 shows the weight change versus time curve recorded during an oxidation test performed at 1600 °C, 800 Pa total pressure, a linear gas flow rate of $10\ \text{m s}^{-1}$ and different oxygen partial pressures. Because the slope corresponding to the second $P^{\text{b}}_{\text{O}_2}$ stage is lower than that obtained in the first stage whereas $P^{\text{b}}_{\text{O}_2}$ increases from 60 Pa to 70 Pa, the transition line has necessarily been crossed (this second stage belongs to the passive oxidation domain). This means that silica has formed on the SiC sample substrate. However, the signal delivered by the microbalance becomes disturbed: it oscillates around an average value which is decreasing with time. The observation of the sample during the experiment has shown the formation and disruption of bubbles in the silica layer.

Two major parameters control the bubble formation in the SiO_2 film: the working total pressure and the physical properties of the oxide layer.

3.2.2.1. Total pressure. To observe bubble formation, the total pressure at the SiC/SiO_2 interface has to be greater than the total pressure in the bulk gas around the silica scale. According to Reaction (14) in (Table IIa), the thermal decomposition of silicon carbide would produce gaseous silicon. Moreover, gaseous species (Si, SiO or SiO_2 and CO or CO_2) would be released after oxidation of SiC by molecular oxygen as depicted by Reactions 15 – 22 in Table IIa. Even if no oxygen is introduced in the furnace, the SiC substrate can react with the SiO_2 layer to form gaseous species according to one (or several) of the reaction equations listed in Table IIc (Reactions 26–31).

If the gaseous products diffuse much more rapidly in the SiO_2 film than the oxidizing reactant (Fig. 12a),

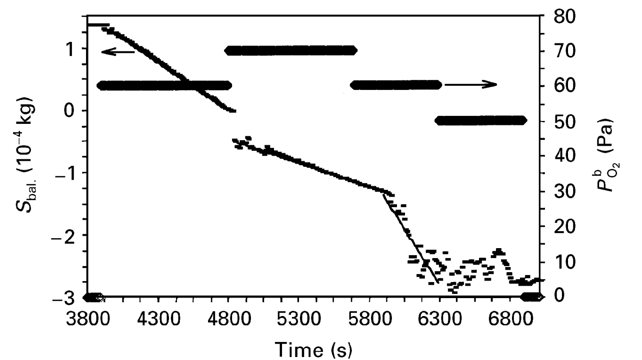

Figure 11 Oxidation at $T = 1600$ °C, $P_{\text{tot}} = 800$ Pa and $V_{\text{gas}} = 10\ \text{m s}^{-1}$ (passive oxidation conditions) of a CVD β-SiC plate. Weight change versus time.

TABLE II The main chemical reactions which involve gaseous product formation at a β-SiC (with possible carbon inclusions) sample surface in an oxidizing (O_2/carrier gas) environment

		Reaction	
(a)	SiC/O_2	$SiC_{(\beta)} \rightleftharpoons Si_{(g)} + C_{(s)}$	(14)
		$SiC_{(\beta)} + \frac{1}{2}O_{2(g)} \rightleftharpoons Si_{(g)} + CO_{(g)}$	(15)
		$SiC_{(\beta)} + O_{2(g)} \rightleftharpoons Si_{(g)} + CO_{2(g)}$	(16)
		$SiC_{(\beta)} + \frac{1}{2}O_{2(g)} \rightleftharpoons SiO_{(g)} + C_{(s)}$	(17)
		$SiC_{(\beta)} + O_{2(g)} \rightleftharpoons SiO_{(g)} + CO_{(g)}$	(18)
		$SiC_{(\beta)} + \frac{3}{2}O_{2(g)} \rightleftharpoons SiO_{(g)} + CO_{2(g)}$	(19)
		$SiC_{(\beta)} + O_{2(g)} \rightleftharpoons SiO_{2(g)} + C_{(s)}$	(20)
		$SiC_{(\beta)} + \frac{3}{2}O_{2(g)} \rightleftharpoons SiO_{2(g)} + CO_{(g)}$	(21)
		$SiC_{(\beta)} + 2O_{2(g)} \rightleftharpoons SiO_{2(g)} + CO_{2(g)}$	(22)
(b)	C/O_2	$C_{(s)} \rightleftharpoons C_{(g)}$	(23)
		$C_{(s)} + \frac{1}{2}O_{2(g)} \rightleftharpoons CO_{(g)}$	(24)
		$C_{(s)} + O_{2(g)} \rightleftharpoons CO_{2(g)}$	(25)
(c)	SiC/SiO_2	$SiC_{(\beta)} + SiO_{2(cond)} \rightleftharpoons 2Si_{(g)} + C_{(s)} + O_{2(g)}$	(26)
		$2\,SiC_{(\beta)} + SiO_{2(cond)} \rightleftharpoons 3Si_{(g)} + 2CO_{(g)}$	(27)
		$SiC_{(\beta)} + SiO_{2(cond)} \rightleftharpoons 2Si_{(g)} + CO_{2(g)}$	(28)
		$SiC_{(\beta)} + SiO_{2(cond)} \rightleftharpoons 2SiO_{(g)} + C_{(s)}$	(29)
		$SiC_{(\beta)} + 2SiO_{2(cond)} \rightleftharpoons 3SiO_{(g)} + CO_{(g)}$	(30)
		$SiC_{(\beta)} + 3SiO_{2(cond)} \rightleftharpoons 4SiO_{(g)} + CO_{2(g)}$	(31)
(d)	C/SiO_2	$2C_{(s)} + SiO_{2(cond)} \rightleftharpoons Si_{(g)} + 2CO_{(g)}$	(32)
		$C_{(s)} + SiO_{2(cond)} \rightleftharpoons Si_{(g)} + CO_{2(g)}$	(33)
		$C_{(s)} + SiO_{2(cond)} \rightleftharpoons SiO_{(g)} + CO_{(g)}$	(34)
		$C_{(s)} + 2SiO_{2(cond)} \rightleftharpoons 2SiO_{(g)} + CO_{2(g)}$	(35)

then no bubble forms in the silica layer, because gases are produced at the SiC/SiO_2 interface at a rate lower than the rate at which they escape, and no overpressure is observed between the SiC/SiO_2 interface and the bulk gas.

In the case illustrated in Fig. 12b, the silica layer would not be an efficient barrier for the oxygen diffusion and oxygen is assumed to have a constant fixed potential at the SiC/SiO_2 interface, equal to $P^b_{O_2}$. Very high quantities of gaseous species could be produced at the SiC/SiO_2 interface (to be in equilibrium with the SiC substrate) and bubbles would form in the silica layer even under atmospheric pressure ($P_{tot} = 0.1$ MPa) whatever the temperature above 1300 °C. But if oxygen could diffuse in the silica layer so that its potential remains constant and equal to $P^b_{O_2}$ at the $SiC–SiO_2$ interface, the kinetics of SiC oxidation would probably be chemically limited and thermodynamic equilibrium would not be reached.

If the oxidation of the SiC substrate is limited by the diffusion in the silica layer of oxygen and/or the gaseous products (Fig. 12c), the partial pressures of the different gaseous products and the resulting total pressure, P^{eq}_{tot}, at the SiC/SiO_2 interface, can be estimated considering the SiC/SiO_2 interface as a close system reacting according to one of the reactions in Table IIa – c. The sum of the partial pressures of the oxygen-containing species at the SiC/SiO_2 interface, balanced with factors related to the stoichiometric coefficients of the considered reaction, is assumed to be equal to $P^b_{O_2}$ (e.g. $P^b_{O_2} = \frac{1}{2}P^{int}_{SiO} + \frac{1}{2}P^{int}_{CO} + P^{int}_{O_2}$ for Reaction 18. Moreover, the partial pressures of the gaseous species at the SiC/SiO_2 interface are related according to their stoichiometric coefficients in the considered reaction (e.g. $P^{int}_{SiO} = P^{int}_{CO}$ for Reaction 18). Thermodynamic data taken from the JANAF tables [14] were used for the calculations. A threshold pressure, P^s_{tot}, has been inferred at each (T; $P^b_{O_2}$) condition and considered to be equal to the most important value of those (P^{eq}_{tot}) calculated independently for the different reactions (Table IIIa). For instance, at $P^b_{O_2} = 10^4$ Pa, this maximum pressure at the SiC/SiO_2 interface is given by Reactions 17 or 18 when the temperature is equal to or lower than 1400 K, by Reaction 15 between 1500 and 1900 K and by Reaction 30 above 2000 K. When the total pressure around the specimen, P_{tot}, is greater than this threshold, P^s_{tot}, the formation of bubbles in the oxide layer is unlikely but it remains possible at lower total pressures. Similar calculations where conducted considering seven other reactions listed in Table IIb and d, which would represent the case of carbon inclusions in the SiC sample. The corresponding results are indicated in Table IIIb.

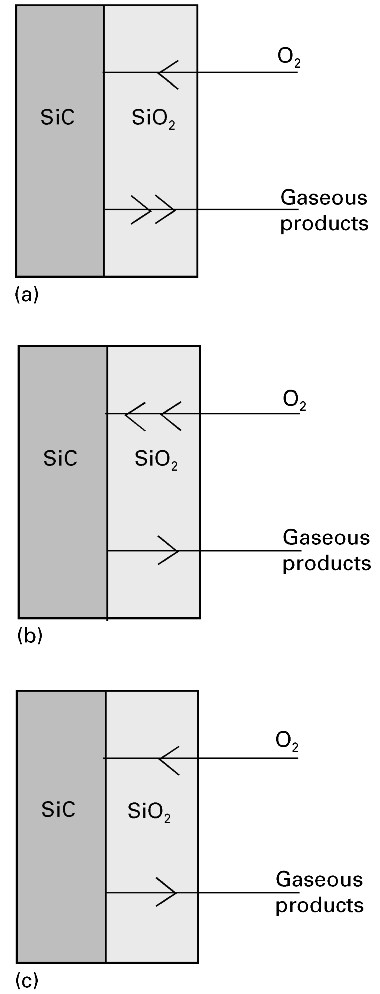

Figure 12 (a–c) Three possible cases considered for the diffusion of gaseous species in the silica layer. (a) Gaseous products diffuse rapidly in the silica layer. No overpressure can appear at the SiC/SiO_2 interface and no bubble is observed in the oxide film. (b) Oxygen diffuses quite rapidly through the silica film such that its potential at the SiC/SiO_2 interface is supposed to be fixed at the given $P^b_{O_2}$ value. (c) Incoming oxygen and outcoming gaseous products diffuse slowly through the silica layer. Gas pressures at the SiC/SiO_2 interface are considered to correspond to equilibrium pressures related to the considered reaction in those listed in Table II.

Experimental conditions investigated by Narushima *et al.* [11], Hinze and Graham [10] and Rosner and Allendorf [9] are located in a $\log(P_{tot})$ $-T^{-1}$–$\log(P^b_{O_2})$ graph and compared to the threshold surface in Fig. 13. Narushima *et al.* [11] and

TABLE III Total pressure threshold values, P^{s}_{tot}, delimiting the region where bubbles can be formed in the silica layer covering a SiC sample

	$P^{b}_{O_2}$																
		Reaction 17 or 18			Reaction 15			Reaction 30					Reaction 34				
	T(K)	10^5	10^4	10^3	10^2	10	1	10^{-1}	10^{-2}	10^{-3}	10^{-4}	10^{-5}	10^{-1}	10^{-2}	10^{-3}	10^{-4}	10^{-5}
(a)	1300	200 000	20 000	2 000	332.84	39.941	3.9531	0.4285	0.4285	0.4285	0.4285	0.4285	2.9594	2.9594	2.9594	2.9594	2.9594
pure	1400	200 000	20 000	2 817.4	399.19	39.941	4.5884	4.5884	4.5884	4.5884	4.5884	4.5884	27.819	27.819	27.819	27.819	27.819
β-sic	1500	200 000	21 476	3 922.1	399.93	39.941	35.548	35.548	35.548	35.548	35.548	35.548	192.60	192.60	192.60	192.60	192.60
	1600	200 000	33 850	3 998.5	399.93	211.84	211.84	211.84	211.84	211.84	211.84	211.84	1 040.5	1 040.5	1 040.5	1 040.5	1 040.5
	1700	232 157	39 579	4 000.0	1 017.3	1 017.3	1 017.3	1 017.3	1 017.3	1 017.3	1 017.3	1 017.3	4 583.8	4 583.8	4 583.8	4 583.8	4 583.8
	1800	331 483	39 981	4 082.4	4 082.4	4 082.4	4 082.4	4 082.4	4 082.4	4 082.4	4 082.4	4 082.4	17 042	17 042	17 042	17 042	17 042
	1900	389 745	39 999	14 087	14 087	14 087	14 087	14 087	14 087	14 087	14 087	14 087	54 933	54 933	54 933	54 933	54 933
	2000	399 053	42 731	42 731	42 731	42 731	42 731	42 731	42 731	42 731	42 731	42 731	156 752	156 752	156 752	156 752	156 752
	2100	399 900	114 565	114 565	114 565	114 565	114 565	114 565	114 565	114 565	114 565	114 565	397 723	397 723	397 723	397 723	397 723
	2200	399 987	279 413	279 413	279 413	279 413	279 413	279 413	279 413	279 413	279 413	279 413	922 754	922 754	922 754	922 754	922 754
	2300	627 729	627 729	627 729	627 729	627 729	627 729	627 729	627 729	627 729	627 729	627 729	1980 962	1980 962	1980 962	1980 962	1980 962
(b)	1300	200 000	20 000	2 000	332.84	39.941	3.9531										
β-sic	1400	200 000	20 000	2 817.4	399.19	39.941	27.819										
containing	1500	200 000	21 476	3 922.1	399.93	192.60	192.60										
carbon	1600	200 000	33 850	3 998.5	1 040.5	1 040.5	1 040.5										
inclusions	1700	232 157	39 579	4 583.8	4 583.8	4 583.8	4 583.8										
	1800	331 483	39 981	17 042	17 042	17 042	17 042										
	1900	389 745	54 933	54 933	54 933	54 933	54 933										
	2000	399 053	156 752	156 752	156 752	156 752	156 752										
	2100	399 900	397 723	397 723	397 723	397 723	397 723										
	2200	922 754	922 754	922 754	922 754	922 754	922 754										
	2300	1980 962	1980 962	1980 962	1980 962	1980 962	1980 962										

Hinze and Graham [10] also studied the active-to-passive oxidation transition of SiC using a microbalance and did not mention any oscillating signal or formation of bubbles in the silica layer: they were working at total pressures higher than the threshold. Rosner and Allendorf [9] worked with CVD β-SiC filament and measured the reduction in diameter of the oxidized specimens but did not study the physical properties of the silica layer possibly formed. However, they were working in conditions where they could have observed bubbles in the silica layer. Mieskowski *et al.* [15] studied the bubble-formation phenomenon in the temperature range 1200–1400 °C at atmospheric pressure (10^5 Pa) during oxidation tests performed on single-crystal (α type) and sintered polycrystalline (α and β type) SiC. Bubbles were observed in the silica layer formed on the surface of the sintered materials oxidized at 1300 °C under 10^5 Pa total pressure, whereas none was found on single-crystal SiC. Their formation were thus thought to arise from carbon inclusions which are common in the sintered materials but rare in SiC single crystal. However, under the conditions investigated by Mieskowski *et al.* [15], the calculated values of P^{s}_{tot} for pure SiC (Fig. 13a) and for a material containing carbon inclusions (Fig. 13b) are equal, which cannot explain the difference experimentally observed.

3.2.2.2. Physical properties of the oxide layer. The second condition necessary for bubbles to form in the silica film concerns some physical properties of the oxide layer. An overpressure has to be established between the two faces of the sample. It implies that the gaseous products cannot escape easily from the SiC/SiO_2 interface. A crystalline SiO_2 film poorly adherent to the SiC substrate and often cracked does not fit these conditions. An amorphous oxide layer held at a temperature greater than that corresponding to the glass transition, T_g, is likely to be blown up by bubbles. That is the case observed at 1600 °C in the present study.

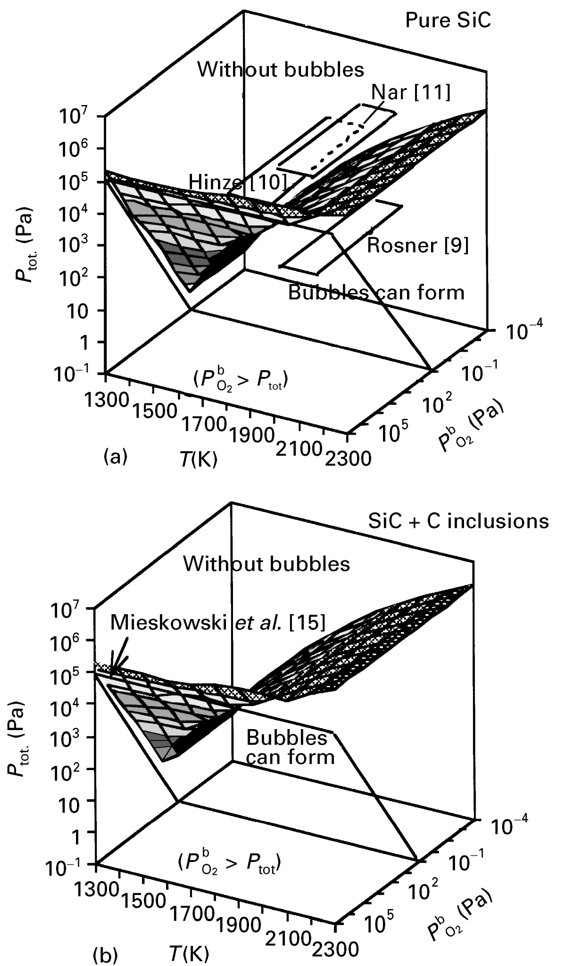

Figure 13 Theoretical surface delimiting the regions were bubbles may or may not form in the silica film which is covering a SiC sample surface. P_{tot}–T–$P^b_{O_2}$ conditions investigated by Narushima *et al.* [11], Hinze and Graham [10], Rosner and Allendorf [9] and Mieskowski *et al.* [15] are also indicated. (a) Pure β-SiC. (b) β-SiC containing carbon inclusions.

3.3. Active oxidation

Fig. 14 shows the relationship between mass loss rate per unit area, $\mathcal{R}$, and oxygen partial pressure in the active oxidation regime ($P^b_{O_2} < P^t_{O_2}$). For given T, P_{tot} and V_{gas} conditions, the experimental ($\mathcal{R}$, $P^b_{O_2}$) points fall into lines approximately starting at zero point ($\mathcal{R} \approx 0$ at $P^b_{O_2} = 0$) indicating then that $\mathcal{R}$ is a linear function of $P^b_{O_2}$. At a linear gas flow rate of 10 m s^{-1}, no significant influence of total pressure on $\mathcal{R}$ is experimentally detected in the range 100–800 Pa. In contrast, $\mathcal{R}$ is greatly affected by an increase of V_{gas} from 10 m s^{-1} to 60 m s^{-1} and this influence depends on temperature. At 1600 °C and 100 Pa total pressure, $\mathcal{R}$ is about five-fold greater for $V_{gas} = 60$ m s^{-1} than for 10 m s^{-1}. Such a dramatic influence of linear gas flow rate on $\mathcal{R}$ implies that the kinetics of active oxidation is controlled by mass transport phenomena under the conditions investigated in this study. An oxidation kinetically controlled

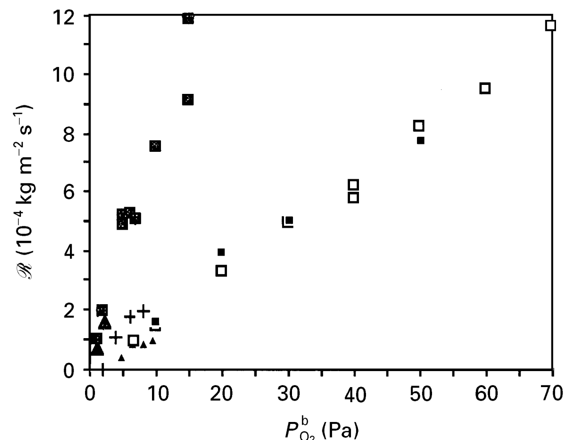

Figure 14 Dependence of weight loss rate per unit area of CVD β-SiC on oxygen partial pressure for different T(°C)–P_{tot} (Pa)–V_{gas} (m s^{-1}) conditions: (△) 1500–100–10, (▲) 1500–800–10, (+) 1500–500–25, (▲) 1500–100–60, (□) 1600–100–10, (■) 1600–800–10, (■) 1600–100–60.

by the chemical reactions at the substrate surface would, in fact, lead to $\mathcal{R}$ values independent of V_{gas}. Narushima *et al.* [16] worked at high temperature, under an atmospheric total pressure (0.1 MPa) and

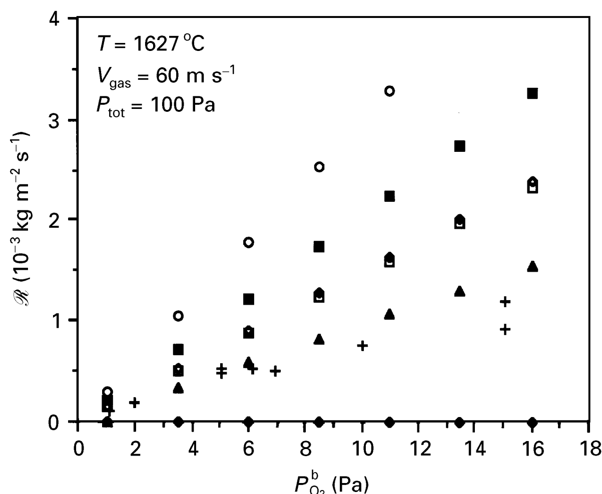

Figure 15 Dependence of calculated mass loss rates per unit area of CVD β-SiC on oxygen partial pressure and comparison with experimental values: (+) Experiment (1600 °C); theoretical Reactions (◆) 14, (○) 15, (◇) 16, (■) 17, (□) 18 and (▲) 19.

low gas flow rate. They observed that $\mathscr{R}$ was a linear function of $P^{\mathrm{b}}_{\mathrm{O_2}}$ and of the square root of temperature. They therefore inferred that the active oxidation of SiC was kinetically controlled by the diffusion of a gaseous species in the gas boundary layer. However, the exact nature of the gaseous species (O_2, CO or SiO) which diffusion limits the active oxidation rate of SiC, cannot be clearly defined, with the only influences of T and $P^{\mathrm{b}}_{\mathrm{O_2}}$ on $\mathscr{R}$.

The mass transport phenomena are thus considered to be the limiting step in the kinetics of active oxidation of SiC. Theoretical mass loss rates per unit area, $\mathscr{R}_{\mathrm{th}}$, of a SiC substrate oxidized according to one of the reactions 14–19 given in Table II, were calculated on this assumption (see Appendix). The results for $T = 1627\,^{\circ}\mathrm{C}$, $P_{\mathrm{tot}} = 100$ Pa and $V_{\mathrm{gas}} = 60\ \mathrm{m\,s^{-1}}$ are presented and compared to experimental values in Fig. 15.

The decomposition of SiC according to Reaction 14 is negligible: it leads to theoretical mass loss rates per unit area very low and independent of $P^{\mathrm{b}}_{\mathrm{O_2}}$ (Fig. 15). The experimental rates are much higher and depend on $P^{\mathrm{b}}_{\mathrm{O_2}}$. Ervin [17] studied the thermal stability of SiC. He also observed that the slightest presence of oxygen significantly increases the removal rate of an SiC sample. This shows how important are the oxidation phenomena in the consumption of an SiC sample which is not only an effect of temperature.

The experimental rates, $\mathscr{R}$, are compared to the closest (i.e. Reactions 17–19) theoretical values, $\mathscr{R}_{\mathrm{th}}$, in Fig. 16a–d. Under the conditions investigated in this study, all the calculated mass loss rates which best fit the experimental values involve the formation of gaseous silicon monoxide. Below 1600 °C (Fig. 16a and b), the mass loss rates per unit area, $\mathscr{R}$, of an SiC sample oxidized at low total pressure (100–800 Pa)

Figure 16 Comparison between experimental, $\mathscr{R}$, and theoretical, $\mathscr{R}_{\mathrm{th}}$, mass loss rates per unit area of a SiC substrate actively oxidized. (a) $\mathscr{R}_{\mathrm{th}}$ corresponds to Reaction 19. (b) $\mathscr{R}_{\mathrm{th}}$ corresponds to Reaction 18. (c) $\mathscr{R}_{\mathrm{th}}$ corresponds to Reaction 18. (d) $\mathscr{R}_{\mathrm{th}}$ corresponds to Reaction 17.

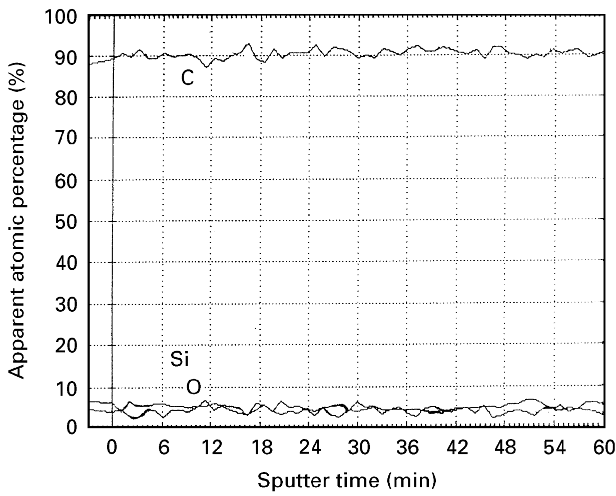

Figure 17 Composition profile determined by AES and argon ion sputtering (18 nm min^{-1} reference Ta_2O_5) of a SiC substrate oxidized at 1700 °C, $P_{tot} = 400$ Pa, $V_{gas} = 36$ m s^{-1} and $P^b_{O_2} = 84$ Pa.

and relatively high linear gas flow rate (10–60 m s^{-1}), are of the order of magnitude of the theoretical rates corresponding to Reactions 18 and 19

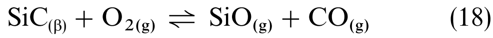

$$SiC_{(\beta)} + O_{2(g)} \rightleftharpoons SiO_{(g)} + CO_{(g)} \qquad (18)$$

and

$$SiC_{(\beta)} + \tfrac{3}{2}O_{2(g)} \rightleftharpoons SiO_{(g)} + CO_{(g)} \qquad (19)$$

When the temperature is about 1700 °C (Fig. 16c and d), $\mathcal{R}$ is of the order of magnitude of $\mathcal{R}_{th}$, related to Reactions 17 and 18

$$SiC_{(\beta)} + \tfrac{1}{2}O_{2(g)} \rightleftharpoons SiO_{(g)} + C_{(s)} \qquad (17)$$

and

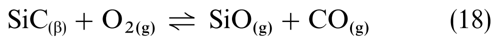

$$SiC_{(\beta)} + O_{2(g)} \rightleftharpoons SiO_{(g)} + CO_{(g)} \qquad (18)$$

To calculate the theoretical rates, the gaseous species are assumed to be in thermodynamic equilibrium at the SiC substrate surface, leading to the maximum partial pressure of gaseous silicon-containing species which can be formed. $\mathcal{R}_{th}$ are, therefore, maximum values. Some experimental rates are higher than theoretical values in Fig. 16a and c. For this reason, below 1600 °C, the main active oxidation reaction of SiC should be

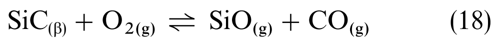

$$SiC_{(\beta)} + O_{2(g)} \rightleftharpoons SiO_{(g)} + CO_{(g)} \qquad (18)$$

and at 1700 °C, in the active oxidation regime, SiC should mainly oxidized according to

$$SiC_{(\beta)} + \tfrac{1}{2}O_{2(g)} \rightleftharpoons SiO_{(g)} + C_{(s)} \qquad (17)$$

In addition, the existence of a carbon layer on the surface of SiC substrates actively oxidized at 1700 °C has been shown by AES analysis (Fig. 17). Although the partial pressure and the gas boundary layer thickness of $SiO_{(g)}$ have been used to calculate $\mathcal{R}_{th}$, the present results cannot allow us to conclude on the exact nature of the gaseous species which diffusion is kinetically limiting the active oxidation of silicon carbide.

4. Conclusion

Experimental (T; $P^t_{O_2}$) transition points were determined at low total pressures (100–800 Pa) and high temperatures (1300–1700 °C). They correspond to conditions for which the mass loss rate per unit area of an SiC substrate is maximum.

In the passive oxidation regime, under low total pressure (100–800 Pa) the silica layer is not uniform on the sample surface and the SiC specimen globally undergoes a mass loss. At high temperatures (e.g. 1600 °C) bubbles form at the SiC–SiO_2 interface disrupting the oxide film.

The mass loss rate per unit area of an SiC sample actively oxidized is a linear function of oxygen partial pressure. It is highly dependent on the linear gas flow rate: the kinetics of active oxidation is controlled by mass transport phenomena under the conditions investigated in this study ($1300\,°C < T < 1700\,°C$, $10 < V_{gas} < 60$ m s^{-1} and $100 < P_{tot} < 800$ Pa). The main reactions of active oxidation of silicon carbide involve the formation of $SiO_{(g)}$ and a release of $CO_{(g)}$ when the temperature is lower than 1600 °C, or the production of $C_{(s)}$ at a higher temperature, typically 1700 °C.

Acknowledgements

This work was supported by SEP and MRES through a grant given to B. Schneider. The authors thank R. E. Tressler, Pennsylvania State University, J. Lahaye, CRPCSS-Mulhouse, and D. Mocaer, SEP-Le Haillan, for valuable discussions, and M. Lahaye, CUMEMSE-UB1, for the AES analyses.

Appendix. Calculations of the mass loss rate per unit area of an SiC specimen actively oxidized in an O_2/inert gas atmosphere

The SiC sample considered for the calculations is a small plate: its thickness, e, is negligible in relation to its length, h, and its width, l The gas flow is parallel to the longest side of the SiC specimen, h, as indicated in Fig. A1.

In active oxidation conditions, silicon carbide oxidizes according to

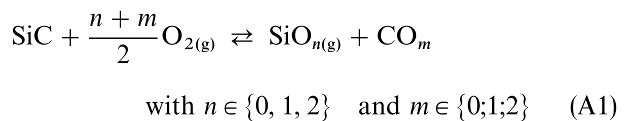

$$SiC + \frac{n+m}{2}O_{2(g)} \rightleftarrows SiO_{n(g)} + CO_m$$

$$\text{with } n \in \{0, 1, 2\} \text{ and } m \in \{0;1;2\} \qquad (A1)$$

The resulting mass loss rate per unit area of the SiC substrate is given by

$$\mathcal{R}_{cons\,SiC} = \frac{M_{SiC}}{hl}\left(\frac{dn_{SiO_n}}{dt}\right)_{z=h} \quad \text{when } m \in \{1;\,2\} \quad (A2a)$$

or

$$\mathcal{R}_{cons\,SiC} = \frac{M_{Si}}{hl}\left(\frac{dn_{SiO_n}}{dt}\right)_{z=h} \quad \text{when } m = 0 \quad (A2b)$$

The reactant gas mixture arriving at the sample (in the plane $z = 0$) is assumed to contain no amount of

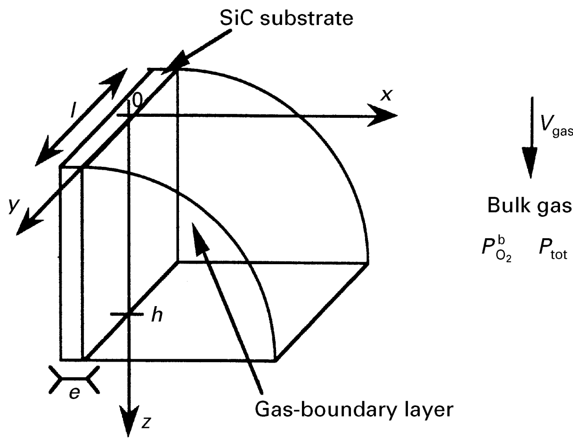

Figure A1

species $SiO_{n(g)}$. During a time dt (infinitely short and such as $dz/dt = V_{gas}$), the mole number of the species SiC which react according to Equation A1 (thereafter leaving the surface of the considered specimen) can be assumed to be equal to the mole number, dn_{SiO_n}, of the gaseous species $SiO_{n(g)}$ which cross the plane $z = h$

$$dn_{SiO_n} = \frac{1}{RT}\int_{y=-\infty}^{\infty}\int_{x=0}^{\infty} P_{SiO_n} dx\, dy\, dz \quad (A3)$$

The $SiO_{n(g)}$ partial pressure, P_{SiO_n}, in the plane $z = h$ is such that

$$\forall x \in]\partial_{SiO_n}; \infty[\qquad P_{SiO_n} \approx 0$$

$$\forall y \in]-\infty; \tfrac{l}{2}[\cup]\tfrac{l}{2}; \infty[\qquad P_{SiO_n} \approx 0$$

Hence

$$dn_{SiO_n} = \frac{1}{RT}\int_{y=-\frac{l}{2}}^{y=\frac{l}{2}}\int_{x=0}^{x=\partial_{SiO_n}} P_{SiO_n} dx\, dy\, dz \quad (A4)$$

According to the gas-boundary layer model, P_{SiO_n} is a linear function of the abscissa x in the range [0; ∂_{SiO_n}]. Its expression further leads to the equation

$$dn_{SiO_n} = \frac{dz}{RT}\int_{y=-\frac{l}{2}}^{y=\frac{l}{2}} dy \int_{x=0}^{x=\partial_{SiO_n}} \left(\frac{P^b_{SiO_n} - P^{int}_{SiO_n}}{\partial^h_{SiO_n}} x + P^{int}_{SiO_n}\right) dx \quad (A5)$$

$$dn_{SiO_n} = \frac{1\,\partial^h_{SiO_n}}{2RT}\left(P^b_{SiO_n} + P^{int}_{SiO_n}\right) dz \quad (A6)$$

The $SiO_{n(g)}$ partial pressure in the bulk gas, $P^b_{SiO_n}$, is negligible in relation to the $SiO_{n(g)}$ partial pressure at the substrate/gas interface, $P^{int}_{SiO_n}$. Thus

$$dn_{SiO_n} = \frac{1\,\partial^h_{SiO_n}}{2RT}(P^{int}_{SiO_n})\, dz \quad (A7)$$

and

$$\frac{dn_{SiO_n}}{dt} \approx \frac{1\,\partial^h_{SiO_n} P^{int}_{SiO_n} V_{gas}}{2RT} \quad (A8)$$

Hence

$$\mathscr{R}_{cons\ SiC} = \frac{M_{SiC}\,\partial^h_{SiO_n} P^{int}_{SiO_n} V_{gas}}{2hRT} \qquad \text{when } m \in \{1; 2\} \quad (A9a)$$

and

$$\mathscr{R}_{cons\ SiC} = \frac{M_{Si}\,\partial^h_{SiO_n} P^{int}_{SiO_n} V_{gas}}{2hRT} \qquad \text{when } m = 0 \quad (A9b)$$

The molar weights of SiC and Si are, respectively, $M_{SiC} = 40.0965\ g\,mol^{-1}$ and $M_{Si} = 28.0855\ g\,mol^{-1}$. The $SiO_{n(g)}$ gas-boundary layer thickness, ∂_{SiO_n}, is calculated as detailed elsewhere [3].

$P^{int}_{SiO_n}$ is calculated considering the following equations.

- When $m \in \{1; 2\}$

$$P^b_{O_2} = P^{int}_{O_2} + \frac{n+m}{2} P^{int}_{SiO_n} \quad (A10a)$$

$$\Delta G^0_{A1} + RT \ln\left[\frac{P^{int}_{SiO_n} P^{int}_{CO_m}}{(P^{int}_{O_2})^{\frac{n+m}{2}}}\right] = 0 \quad (A10b)$$

$$P^{int}_{SiO_n} = P^{int}_{CO_m} \quad (A10c)$$

- When $m = 0$

$$P^b_{O_2} = P^{int}_{O_2} + \frac{n+m}{2} P^{int}_{SiO_n} \quad (A11a)$$

$$\Delta G^0_{A1} + RT \ln\left[\frac{P^{int}_{SiO_n}}{(P^{int}_{O_2})^{\frac{n+m}{2}}}\right] = 0 \quad (A11b)$$

ΔG^0_{A1} is the standard Gibbs energy of Reaction A1.

References

1. N. S. JACOBSON, *J. Am. Ceram. Soc.* **76** (1993) 3.
2. J. A. COSTELLO and R. E. TRESSLER, *ibid.* **69** (1986) 674.
3. B. SCHNEIDER, A. GUETTE, C. BERNARD, P. ROCABOIS and M. CATALDI, *J. Eur. Ceram. Soc.*, to be submitted.
4. B. SCHNEIDER, A. GUETTE, J. THÉBAULT, M. CATALDI and R. E. TRESSLER, *ibid.*, to be submitted.
5. W. F. McCLUNE, T. M. MAGUIRE, B. POST, S. WEISSMAN, H. F. McMURDIE, L. ZWELL and M.C. MORRIS, "Powder Diffraction File – Inorganic Phases" (JCPDS International Centre for Diffraction Data Swarthmore, PA, 1990).
6. L. H. KEYS, in "The Oxidation of Silicon Carbide", Proceedings of the Symposium on Properties of High Temperature Alloys, Vol. **77-1**. (The Electrochemical Society, Princeton, NJ, 1977) pp. 681–96.
7. T. NARUSHIMA, T. GOTO, Y. YOKOYAMA, J. HAGIWARA, Y. IGUSHI and T. HIRAI, *J. Am. Ceram. Soc.* **77** (1994) 2369.
8. W. C. TRIPP and H. C. GRAHAM, *ibid.* **59** (1976) 399.
9. D. E. ROSNER and H. D. ALLENDORF, *J. Phys. Chem.* **74** (1970) 1829.
10. J. W. HINZE and H. C. GRAHAM, *J. Electrochem. Soc.* **123** (1976) 1066.
11. T. NARUSHIMA, T. GOTO and T. HIRAI, "Active-to-Passive Transition in the Oxidation of CVD-SiC", Proceedings of the International Meeting on Advanced Materials, **4** Materials Research Society, Pittsburgh, P.A. (1989) 295.
12. E. A. GULBRANSEN, K. F. ANDREW and F. A. BRASSART, *J. Electrochem. Soc.* **113** (1966) 1311.

13. B. BERTON, M. P. BACOS, D. DEMANGE and J. LAHAYE, *J. Mater. Sci.* **27** (1992) 3206.
14. M. W. CHASE Jr, C. A. DAVIES, J. R. DOWNEY Jr, D. J. FRURIP, R. A. McDONALD and A. N. SYVERUD, JANAF Thermochemical Tables, 3rd Edn., Edited by M. W. Chase Jr., C. A.Davies, J. R. Dowrey Jr., D. J. Frurip and A. N. Syverud, American Chemical Society and The American Institute of Physics for the National Bureau of Standards, New York *J. Phys. Chem. Ref. Data*, **14** Suppl.1 (1985)
15. D. M. MIESKOWSKI, T. E. MITCHELL and A. H. HEUER, *J. Am. Ceram. Soc.*, **67** (1).
16. T. NARUSHIMA, T. GOTO, Y. IGUSHI and T. HIRAI, *J. Am. Ceram. Soc.* **74** (1991) 2583.
17. G. ERVIN, *ibid.* **41** (1958) 347.

Received 23 October 1995
and accepted 24 April 1996